Gate Tunable Magneto-resistance of Ultra-Thin WTe_2 Devices

Xin Liu[1*], Zhiran Zhang[1], Chaoyi Cai[1], Shibing Tian[1], Satya Kushwaha[2], Hong Lu[1], Takashi Taniguchi[3], Kenji Watanabe[3], Robert J. Cava[2], Shuang Jia[1,4*], Jian-Hao Chen[1,4*]

[1] International Center for Quantum Materials, Peking University, Beijing 100871, China

[2] Department of Chemistry, Princeton University, Princeton, USA

[3] High Pressure Group, National Institute for Materials Science, 1-1 Namiki, Tsukuba, Ibaraki 305-0044, Japan

[4] Collaborative Innovation Center of Quantum Matter, Beijing 100871, China

[*]Xin Liu (liux23@pku.edu.cn), Shuang Jia (jiashuang@gmail.com) and Jian-Hao Chen (chenjianhao@pku.edu.cn)

PACS: 72.80.Ga; 73.43.Qt

Keywords: transition metal dichalcogenide; electronic device; solid-dielectric gate; magneto-resistance

Abstract: In this work, the magneto-resistance (MR) of ultra-thin WTe_2/BN heterostructures far away from electron-hole equilibrium is measured. The change of MR of such devices is found to be determined largely by a single tunable parameter, i.e. the amount of imbalance between electrons and holes. We also found that the magnetoresistive behavior of ultra-thin WTe_2 devices is well-captured by a two-fluid model. According to the model, the change of MR could be as large as 400,000%, the largest potential change of MR among all materials known, if the ultra-thin samples are tuned to neutrality when preserving the mobility of 167,000 $cm^2V^{-1}s^{-1}$ observed in bulk samples. Our findings show the prospects of ultra-thin WTe_2 as a variable magnetoresistance material in future applications such as magnetic field sensors, information storage and extraction devices, and galvanic isolators. The results also provide important insight into the electronic structure and the origin of the large MR in ultra-thin WTe_2 samples.

Introduction

1T'-Tungsten ditelluride (WTe_2) is a layered transition metal dichalcogenide (TMDC) with a distorted structure that preserves inversion symmetry in the out-of-plan direction, contrasting with TMDCs with 2H phases, such as 2H-MoS_2 [1]. The material in its pristine bulk form is a semimetal [2, 3]. It exhibits rich physics such as extraordinarily large and non-saturating magneto-resistance (XMR) [4], superconductivity under high pressure [5, 6], and may be a type-II Weyl semimetal (WSM) at a particular level of electron doping [7-10]. Furthermore, reports on thin films of WTe_2 show the tunability of magnetoresistance revealing interesting new phenomena such as the transition from weak anti-localization to weak localization [11], the depletion of holelike carriers in the suppressed-MR regime [12], long-range field effect [13], the topological insulator-like behavior [14], and negative longitudinal MR indicating WTe_2 a type-II WSM [15]. The origin of the XMR in WTe_2, together with its potential

application in magnetic field sensing and in information storage, has attracted much attention in the scientific and technical community [16-21]. The majority of the research in XMR has been carried-out in bulk WTe_2 samples with near-perfect electron-hole compensation, and the results support the picture that the XMR arises from such near-perfect compensation of electrons and holes [17], i.e. a two-fluid picture. However, electrolyte gating experiments on thinner WTe_2 samples (~70nm) have shown non-saturating XMR that deviates from the two-fluid theory [18]. Here, we have carried out careful experiments with solid-dielectric gated ultra-thin WTe_2 samples (~10nm) that are far away from charge neutrality. We find that in this regime, the MR of the samples can still be well explained by the two-fluid model, and the sample shows 2D weak anti-localization effects at low temperatures. We also found that the change of MR of the ultra-thin WTe_2 is determined largely by the density difference between the electron and hole carriers, pointing to possible future application of this material in electric-field tunable, variable sensitivity magnetic field sensors [22-24].

Device fabrication and measurement

The ultra-thin WTe_2 samples measured in this letter are mechanically exfoliated from bulk WTe_2 crystal and transferred on to thin h-BN single crystals placed on 300nm SiO_2/Si substrates [25]. We found that using single crystal BN substrates resulted in an increase in the mobility of our samples which are 10nm thick or less (see section S4 at Supporting information for details). WTe_2 bulk crystals are synthesized using chemical vapor transport technique [4] and h-BN bulk crystals are grown by the method described in ref. [26]. The thin h-BN (thickness～15nm) surface is free of dangling bonds, greatly alleviates the influence of surface charge traps in the SiO_2 layer, and could substantially improve quality of low-dimensional devices. Standard electron-beam lithography technique is used to pattern electrodes, consisting of 6nm Cr and 60nm Au, on the WTe_2 samples to form multi-terminal field effect devices (FEDs). We have taken particularly careful measures to ensure that the samples do not expose to ambient conditions at all. The sample preparation process, device fabrication process and electrical transport measurement are done in inert atmosphere, or with the sample capped with a protection layer. The protection layer consists of 200 nm thick polymethyl methacrylate (PMMA) or a bilayer of 200 nm PMMA and 200 nm MMA. Electrical- and magneto-transport measurements were carried out in a Quantum Design PPMS-9 with standard lock-in technique.

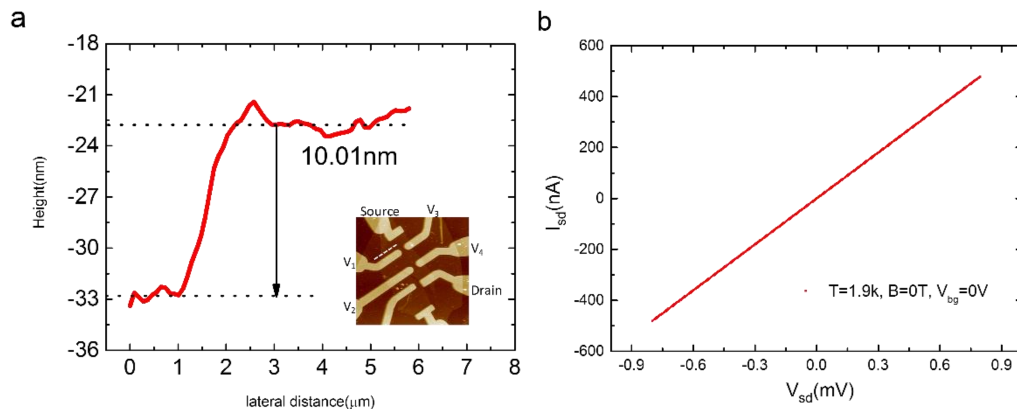

Figure 1 Few-layer WTe_2 FET device characteristics. **(a)** Thickness of the WTe_2 FET device measured by atomic force microscopy (AFM). Inset shows the AFM micrograph of the device. The channel length (between V_1 and V_2) and width are 3.9 μm and 1 μm, respectively. The white dashed line in the inset panel marks the cross-section of the sample in (a). **(b)** Two-terminal I_{sd}-V_{sd} characteristics of the device at T=1.9K without magnetic field and at zero back gate voltage.

We shall focus our discussion on one device (sample A) in the main text; data for other WTe_2 devices are shown in supporting information. An atomic force microscopy (AFM) micrograph of a 10nm-thick WTe_2 device as well as its height section profile is shown in figure 1a. Figure 1b shows the *I*-*V* characteristics of the WTe_2 field effect device at 1.9 Kelvin under zero magnetic field and zero back gate voltage, measured with two-probe configurations (between source and drain electrodes shown in the inset of figure 1a). The source-drain current (I_{sd}) varies quite linearly with the applied voltage V_{sd} from -0.8mV to 0.8mV, with resistivity of $4.26 \times 10^{-4}\Omega\cdot$cm, indicating an Ohmic contact to a metallic sample. Raman spectra of the device (see section S3 in supporting information) obtained in a Horiba Jobin Yvon LabRam HR Evolution system after the transport experiments showed that the WTe_2 sample is indeed in the 1T' phase [27] and has not degraded.

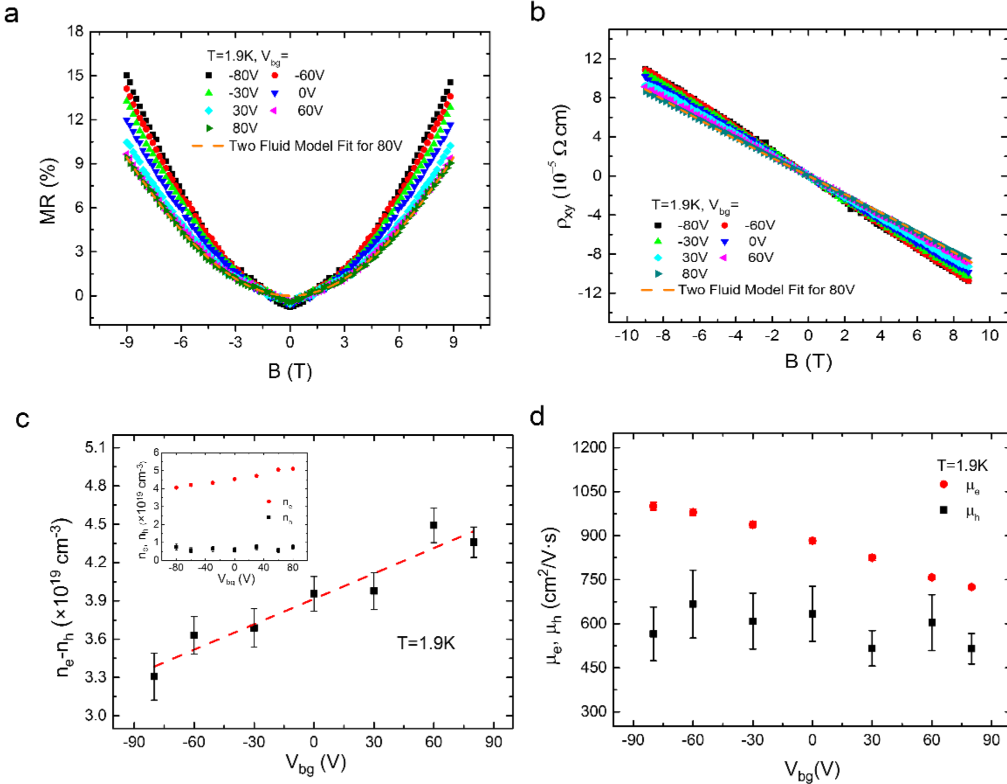

Figure 2 Gate-dependent behavior in WTe_2 thin flake. **(a)**, **(b)** Gate dependence of MR and ρ_{xy} at T=1.9K. The colors mark different back gate voltage. Dashed lines are fits to the two-fluid model for MR and ρ_{xy} at V_{bg}=80V. **(c)**, **(d)** Gate dependence of net carrier density (n_e-n_h) and mobility for electrons and holes. Dashed line in (c) is a linear fit to the data. Inset

figure in (c) shows electron and hole density as a function of back gate voltage, respectively.

Magneto-transport mechanism of WTe_2 FET devices

Figures 2a and 2b show the longitudinal magneto-resistance $MR(B) = (\rho_{xx}(B) - \rho_{xx}(B=0))/\rho_{xx}(B=0)$ and Hall resistance ρ_{xy} of the sample at T=1.9K, with the magnetic field applied perpendicular to the sample surface (along the c axis), and at different back gate voltages. All measurements of magnetoresistance are done in four-probe configurations to eliminate contact effects. The sample exhibits a positive $MR(B)$ and quasi-linear $\rho_{xy}(B)$ under all the gate voltages investigated in this experiment. For small magnetic field, $MR(B)$ has a cusp-shape which will be discussed later. For magnetic fields larger than 1 Tesla, $MR(B)$ can be fitted by a power law behavior, $MR \propto B^{\gamma}$, with the exponent γ between 1.62 and 1.69 for different gate voltages, which is smaller than the exponent γ~1.94 observed in an 112nm-thick sample (see section S1 in supporting information), and smaller than the exponent γ~2 observed bulk crystals [4]. We will show later in this report that weak anti-localization should be taken into account (see figure 6) and the exponent γ is not a constant of magnetic field for electron-hole uncompensated samples (see section S7 in supporting information).

It has been found by transport [28-30] and ARPES [16, 17, 31, 32] experiments that bulk WTe_2 crystals have 4-9 carrier pockets; however, researchers are just starting to examine how these pockets evolve as the sample is getting thinner [33]. Here we started out to analyze the data with the ansatz that there are two major types of carriers in the sample, one type is electrons and the other type is holes. We will show that this ansatz captures the majority of the physics in the high field magnetoresistance of ultra-thin WTe_2 samples, and that it is also consistent with low field magnetoresistance data.

In a two-fluid model [34], we have

$$\rho_{xx} = \frac{1}{e}\frac{(n_e u_e + n_h u_h) + (n_e u_h + n_h u_e) u_e u_h B^2}{(n_e u_e + n_h u_h)^2 + \left((n_e - n_h) u_e u_h B\right)^2}$$

(1)

$$\rho_{xy} = \frac{1}{e}\frac{\left(n_e \mu_e^2 - n_h \mu_h^2\right) - (n_h - n_e)\mu_e^2 \mu_h^2 B^2}{(n_e u_e + n_h u_h)^2 + \left((n_h - n_e) u_e u_h B\right)^2} B$$

(2)

$$\mathrm{MR} = \frac{\rho_{xx}(B) - \rho_{xx}(B=0T)}{\rho_{xx}(B=0T)} = \frac{\frac{n_h}{n_e}(u_e + u_h)^2 u_e u_h B^2}{\left(u_e + \frac{n_h}{n_e} u_h\right)^2 + \frac{n_h}{n_e}\left(\left(\frac{n_h}{n_e} - 1\right) u_e u_h B\right)^2}$$

(3)

where n_e (n_h) and u_e (u_h) are carrier density and mobility for electrons (holes), respectively. At all the gate voltages, both the MR and ρ_{xy} of the ultra-thin device can be simultaneously fitted by equation (3) and (2), and n_e, n_h, u_e, u_h can be extracted from the fit. Using the least squares method, we determine the values of the four parameters with minimum error (see section S9 in supporting information for details).

Figure 2c shows the net charge carrier density $n=n_e-n_h$ as a function of V_g, and the dashed line is a linear fit to the data. The induced charge in the sample by the silicon back gate is: $ne = C_g \Delta V_g$, where e is the elementary charge and C_g is the parallel-plate capacitance of the device per unit area. Thus from the linear fit, we obtained a gate capacitance of $C_g = 1.062 \times 10^{-4}\, F/m^2$. Since the dielectric in our device consists of 15nm of h-BN (relative permittivity $\epsilon_{h-BN} \approx 3.5$) and 300nm of SiO_2 ($\epsilon_{SiO_2} \approx 3.9$), one can get the series capacitance for this multilayer system to be $C_g' = \left(\frac{1}{C_g^{h-BN}} + \frac{1}{C_g^{SiO_2}}\right)^{-1} = 1.089 \times 10^{-4}\, F/m^2$, in good agreement with our experimental data. The above analysis show that the longitudinal magnetoresistance of the device can be tuned electrostatically and that the phenomenological two-fluid model captures the main feature of the magneto-transport properties of our ultra-thin WTe_2 samples. Note that the ultra-thin samples in this study are predominately electron-doped, with electron densities 5-10 times larger than hole densities; in comparison, thicker samples (the 112nm-thick sample, see section S1 in supporting information) exfoliated from the same bulk crystal are found to be close to charge neutrality. The imbalance between electrons and holes in the ultra-thin devices are likely due to unintentional doping from the device fabrication process; such imbalance also allows us to access the highly electron-doped regime in ultra-thin WTe_2 samples to test the applicability of the two-fluid model [4, 18].

Figure 2d shows the gate-dependent mobility for electrons and holes. We note that the electron mobility decreases as the density becomes larger at T=1.9K, suggesting that charged impurities are not the dominating scattering source in this regime [35]. From figure 2d as well as from the inset of figure 2c, we find that n_e and u_e are being effectively tuned by the gate voltage while n_h and u_h are much less affected by V_g, which is likely caused by the fact that the density of states of electrons is much larger than that of holes in this highly electron-doped regime.

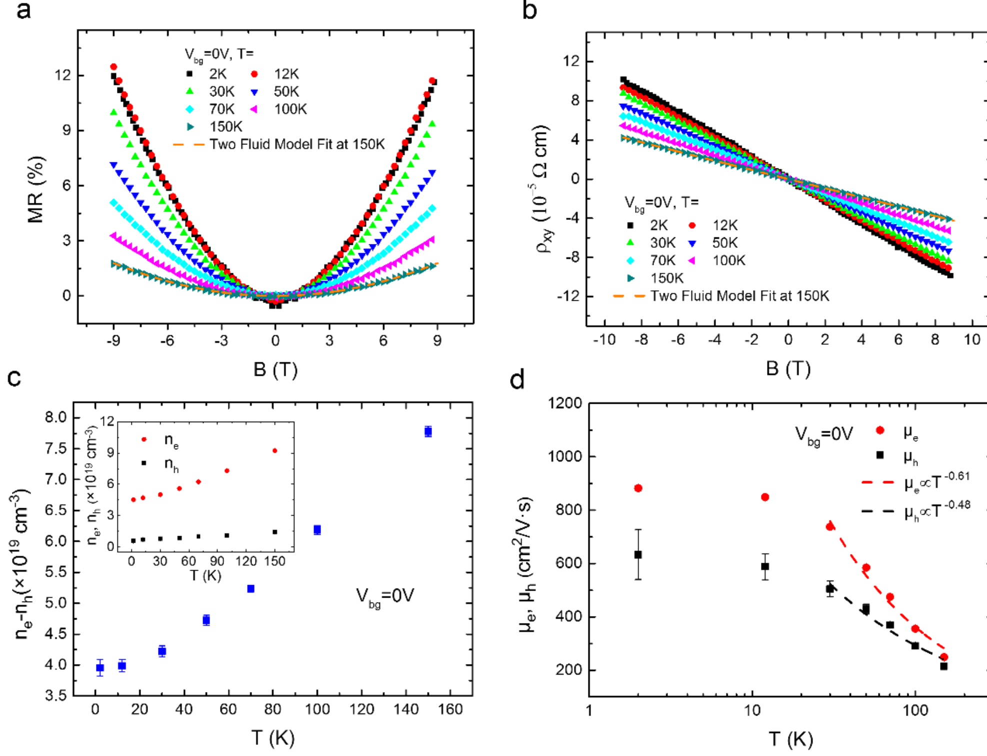

Figure 3 Temperature-dependent behavior of a WTe_2 ultra-thin flake device. **(a)**, **(b)** *MR* and Hall resistivity as a function of magnetic field at different temperatures at V_{bg}=0V. Dashed lines are fit curve to the two-fluid model for *MR* and ρ_{xy} at 150K. **(c)**, **(d)** Temperature dependence of net charge carrier density (n_e-n_h) and the mobility of electrons and holes at V_{bg}=0V. The inset panel in (c) shows electron and hole density vs. temperature. Dashed lines in (d) are power law fits for $\mu \propto T^{-\gamma}$, with the exponents γ≈0.61 and 0.48 for electrons and holes, respectively.

Figures 3a and 3b show the temperature-dependent *MR* and ρ_{xy} of the device from T=1.9K to 150K and at zero gate voltage. The cusp-shape in *MR* at small magnetic field diminishes rapidly as the temperature increases, and will be discussed in detail later. At magnetic field larger than two Tesla, fitting the *MR* by a power law behavior $MR \propto B^{\gamma}$ results in a temperature-dependent exponent γ that changes from ~1.69 at T=1.9K to 2 at T=150K. At the meantime, ρ_{xy} remains linear in B with its slope k changes monotonically at different temperatures. We are going to show in this letter that such temperature-dependence of γ and k is also well captured by the phenomenological two-fluid model.

Similar to the analysis of the gate dependent magnetoresistance, the *MR* and ρ_{xy} of the device at different temperatures are fitted simultaneously by equation (3) and (2), and the dependencies of n_e, n_h, u_e, u_h on temperature are extracted from the fit. Figure 3c shows the dependence of the net carrier charge n_e-n_h as a function of temperature. It can be seen that by lowering the temperature, the sample rapidly tends to its charge neutrality on cooling from 150K to 50K; the trend slows down below 50K and saturates from 12K to 1.9K. The mobilities u_e and u_h, on the other hand, increase following a power law of $\mu \propto T^{-\alpha}$ from

150K to 50K and then saturate from 12K to 1.9K. This suggests a connection between the decrease in n_e-n_h and the increase of u_e and u_h, which is consistent with the carrier density dependent measurements at a fixed temperature. Temperature-dependent movement of chemical potential has been seen in multiple semimetal bulk crystals [31, 36-38], and has been attributed to be the cause of a temperature-induced Lifshitz transition for WTe_2 bulk crystals [31]. Thus it is not surprising to see such temperature-dependent n_e-n_h in ultra-thin WTe_2 samples. A fit to a power law behavior of the decreasing mobility with increasing temperature give an exponent α for electrons (α=0.61) and holes (α=0.48); these values are similar to those for few-layer black phosphorus [39] and dual-gated monolayer MoS_2 [40]. However, they are smaller than the theoretically predicted value (α~1.52) [41] and smaller than our experimental data obtained from bulk WTe_2 samples (α~1.30 to 1.51) (see section S2 in supporting information). The suppression of α is considered to be caused by a quenching of the characteristic homopolar mode in sandwiched ultra-thin device structures [40]. In the case of WTe_2, this means that ultra-thin samples can preserve their mobility, thus preserving their response to magnetic field, much better than their bulk counterparts at room temperature (see section S2 in supporting information), which is good for technological applications.

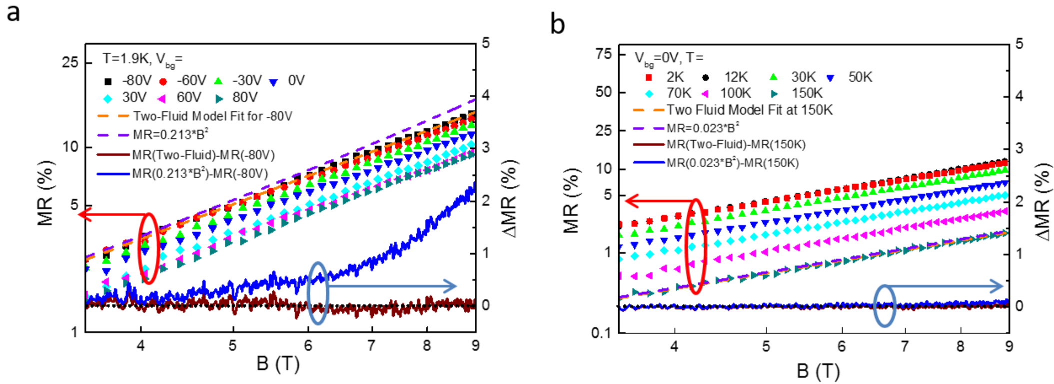

Figure 4 (a) Gate-voltage dependent *MR* plotted on a log-log scale. The orange dashed lines are the two-fluid model fit to the *MR* at V_g = -80 volts at T=1.9K, the purple dashed line is a B^2 MR curve as a guide to the eye; the blue solid line is the difference between the MR data at V_g = -80 volts at T=1.9K and the B^2 behavior, while the wine solid line is the difference of the same data to the prediction of the two fluid model. **(b)** Temperature dependent MR plotted on a log-log scale. The orange dashed lines are the two-fluid model fit to the MR at V_g = 0 volts at T=150K, the purple dashed line is a B^2 MR curve as a guide to the eye; the blue solid line is the difference between the MR data and the B^2 behavior, while the wine solid line is the difference between the same data and the prediction of the two fluid model.

Since the ultra-thin WTe_2 sample is not at the charge neutral point, we expect a saturation of magnetoresistance for high enough magnetic field, if the transport behavior of the sample follows the two-fluid model. Indeed, if we look closely into the *MR* curves, we confirm such saturation at high magnetic field. Figures 4a and 4b show the gate-voltage dependent *MR* and

temperature dependent *MR* plotted in log-log scale. It can be seen that for all the gate voltages we applied at 1.9K, the *MR* of the sample deviates from the ~B^2 functional form, while conforming to the prediction of the two-fluid model. In figure 4a, the blue solid line is the difference between the MR data at V_g = -80 volts at T=1.9K and the B^2 behavior, while the wine solid line is the difference of the same data to the prediction of the two fluid model. A deviation from the B^2 behavior (e.g., the saturation of *MR* at high magnetic field) is clearly observed. At higher temperature, the mobility of the carriers drops much faster than the increase in the net charge density of the sample, leading to a higher saturation magnetic field, which is out of the range of our experimental apparatus. Thus the MR data at 150K fits the two-fluid model and a scaled B^2 functional form equally well (figure 4b).

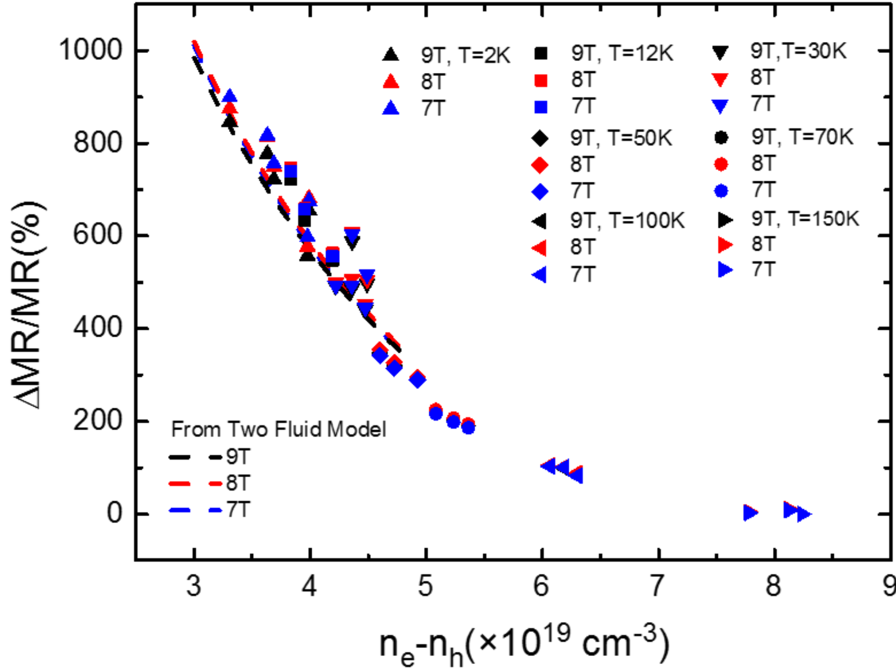

Figure 5 Tunable MR by carrier density in a WTe_2 ultra-thin flake device. Charge carrier density dependence of normalized magneto-resistance, defined as $(MR(n)-MR(n_0))/MR(n_0)$, where $n = n_e-n_h$ is the net charge density and $n_0 = 8.2 \times 10^{19}\text{cm}^{-3}$ is the largest net charge density measured in this device. Dashed lines are the two-fluid model prediction of $MR(n_e-n_h)$ curves for magnetic field of 7T, 8T and 9T.

Figure 5 is one of the primary observations of our study. It shows the change of *MR* as a function of n_e-n_h at three different magnetic fields (7T, 8T, 9T) and at all temperatures from 150K to 1.9K. (The change of *MR* is defined as $(MR(n)-MR(n_0))/MR(n_0)$, where $n = n_e-n_h$ is the net charge density and $n_0 = 8.2 \times 10^{19}\text{cm}^{-3}$ is the largest net charge density measured in our experiment, at T = 150K.) It can be seen that the change of *MR* increases monotonically as n_e-n_h decreases, regardless of temperature and magnetic field. The two-fluid model predicted $MR(n_e-n_h)$ curves for magnetic field of 7T, 8T and 9T are also shown in figure 4, showing

similar insensitivity to the magnetic field applied. This property of ultra-thin WTe_2 devices is very useful in making future tunable sensitivity magnetic field sensors, where a universal dependence on a single parameter (net charge carrier) is preferred. It is worth noting that such a curve is empirical, and it is a useful derivation from the two-fluid model. Experimentally, we found that for the carrier mobility about 1000 cm^2/Vs or lower, and for magnetic field 9T or lower, such single-parameter dependence of ΔMR on n_e-n_h holds pretty well.

The largest change of *MR* measured in our experiment is 850%, in which the 2D electron-hole imbalance is tuned from $8.2 \times 10^{19}cm^{-3}$ to $3.2 \times 10^{19}cm^{-3}$. If we reached charge neutrality in this particular device, the change of MR could be 8,400% (see section S8 in supporting information for the calculation). Furthermore, as fabrication techniques improve, we expect the mobility of ultra-thin WTe_2 devices to finally approach that of bulk crystals. (Such rapid improvement of device fabrication techniques has been seen in the field of graphene, where it did not take a long time for the mobilities of graphene devices to improve from 10,000cm^2/Vs [42] to 1,000,000cm^2/Vs [25].) Using a fixed mobility value of 1.67×10^5 $cm^2V^{-1}s^{-1}$ from Ref. [43] for both *MR*(p/n=1) and *MR*(p/n=0.1559), we project a change of *MR* of 400,000%. Note that this should be a lower bound for the estimation, as the mobility at the neutrality point should be much higher than when p/n=0.1559 (see figure 2d and supporting information for more details). Thus we expect ultra-thin WTe_2 to be a very useful electric-field-tuned magnetoresistance material in future technological applications.

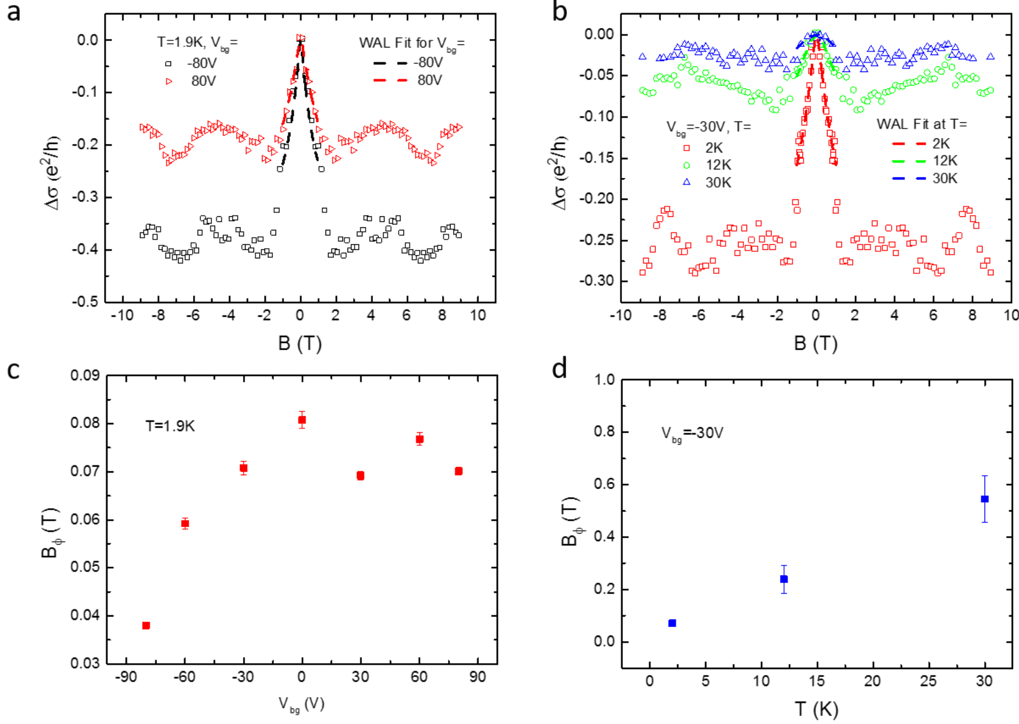

Figure 6. WAL in WTe_2 thin flake. **(a)** The change of conductance $\Delta\sigma_{xx}(B) = \sigma_{xx}(B)$-$\sigma_{xx}(B=0)$ of the ultra-thin WTe_2 device at T = 1.9K at largest gate voltages $V_g = \pm 80$ volts. **(b)** $\Delta\sigma_{xx}(B)$ curves for T = 2K, 12K and 30K at gate voltage V_g = -30 volts. The dashed lines in (a) and (b) are weak anti-localization fit to the data between ±1T of magnetic field. **(c)**&**(d)** Phase related field B_ϕ as a function of back gate voltage at T = 1.9K (c) and at different temperatures at V_g

= -30 volts (d).

Continuing the analysis of our observations, figure 6a shows the change of conductance $\Delta\sigma_{xx}(B) = \sigma_{xx}(B)-\sigma_{xx}(B=0)$ of the ultra-thin WTe_2 device at T = 1.9K, after subtracting the classical contribution determined by the two-fluid model, and for the largest gate voltages (V_g = ±80 volts) applied in experiment. The low field magneto-conductance shows a peak that can be strongly modified by the gate voltage. Figure 6b shows the $\Delta\sigma_{xx}(B)$ curves for T = 2K, 12K and 30K, with V_g = 30 volts. It can be seen that the low field magneto-conductance diminishes rapidly as T increases. Above 30K, the peak in low field magneto-conductance can no longer be detected. The magnitude and the temperature dependence of the low field magneto-conductance are characteristics of two-dimensional weak anti-localization, similar to previously reported result in ultra-thin WTe_2 devices [15, 19]. We fit our experimental data to the Hikami-Larkin-Nagaoka (HLN) equation [44]:

$$\Delta\sigma_{xx}(B) = -\frac{e^2}{2\pi^2\hbar}\left[\psi\left(\frac{1}{2}+\frac{B_\phi}{B}\right) - ln\left(\frac{B_\phi}{B}\right) - 2\psi\left(\frac{1}{2}+\frac{B_\phi+B_{so}}{B}\right) + 2ln\left(\frac{B_\phi+B_{so}}{B}\right) - \psi\left(\frac{1}{2}+\frac{B_\phi+2B_{so}}{B}\right) + ln\left(\frac{B_\phi+2B_{so}}{B}\right)\right] \quad (4)$$

where ψ is the digamma function, $B_n = \frac{\hbar}{4el_n^2} = \frac{\hbar}{4eD\tau_n}, n = \phi, so$ is the characteristic field related to phase coherence length (time) l_ϕ (τ_ϕ) and spin-orbit interaction terms. D is the diffusion constant. In small magnetic field (B<1T), we find B_{so} is too large to affect $\Delta\sigma_{xx}(B)$. Hence, following the literature, we fitted $\Delta\sigma_{xx}(B)$ curves by setting B_{so}=6T [19]. Figure 6c shows the dependence of the fitting parameter B_ϕ on V_g at T=1.9K. It can be seen that B_ϕ drops by 50% if V_g changes from 80 volts to -80 volts, indicating a significant increase in the phase coherence length of charge carriers as the sample tends to charge neutrality, consistent with the magnetoresistance data at higher magnetic field. B_ϕ increases linearly with temperature, which could be a manifestation of strong electron-electron interaction in the material [19, 45, 46].

Conclusion

In summary, we have fabricated ultra-thin WTe_2 field effect devices with solid gate dielectrics, and found that in electron-dominated regime, ultra-thin WTe_2 samples have a gate tunable magnetoresistance that is consistent with the two-fluid model. We estimate that the value of $\Delta MR/MR$ could be as high as 400,000% within experimentally accessible parameters, a value much higher than other materials. The tunability of MR by a single parameter (the net charge density $n=n_e-n_h$) together with the insensitivity of $\Delta MR/MR$ to magnetic field and temperature, reveal the potential of ultra-thin WTe_2 as electric-field-tuned magnetoresistance material which could have important application in magnetic field sensing, information storage and extraction, and galvanic isolation.

Acknowledgement

This project has been supported by the National Basic Research Program of China (973 Grant Nos. 2013CB921900, 2014CB920900), and the National Natural Science Foundation of China (NSFC Grant Nos. 11374021) (X. Liu, Z. Zhang, C. Cai, S. Tian, H. Lu, S. Jia, J.-H. Chen). K.W. and T.T. acknowledge support from the Elemental Strategy Initiative conducted by the MEXT, Japan and a Grant-in-Aid for Scientific Research on Innovative Areas “Science of Atomic Layers” from JSPS. The work at Princeton University was supported by the ARO MURI on topological insulators, grant W911NF-12-1-0461.We are grateful to Professor Alberto Morpurgo for inspiring discussions.

Author Contributions

X.L. and J.C. conceived the experiment. X.L. exfoliated the WTe_2 thin flakes and few-layer h-BN crystals and accomplished the heterojunction FET devices fabrication. S.K, H.L., S.J. and R. J. C. grew WTe_2 bulk crystals; T.T. and K.W. grew h-BN bulk crystals. X.L., C.C and S.T. performed the transport measurements and Raman measurements. X.L., C.C, Z.Z. and J.C. discussed the results and analyzed the data. X.L. and J.C. wrote the manuscript and all authors commented on it.

Reference:

[1] L F Mattheiss 1973 Band Structures of Transition-Metal-Dichalcogenide Layer Compounds *Phys. Rev. B* **8** 3719-3740.

[2] S Kabashima 1966 Electrical properties of Tungsten-Ditelluride WTe_2 *J. Phys. Soc. Jpn* **21** 945.

[3] J Augustin, V Eyert, T Böker, W Frentrup, H Dwelk, C Janowitz, R Manzke 2000 Electronic band structure of the layered compound Td-WTe_2 *Phys. Rev. B* **62** 10812.

[4] M N Ali, et al. 2014 Large, non-saturating magnetoresistance in WTe_2 *Nature* **514** 205.

[5] X-C Pan, et al. 2015 Pressure-driven dome-shaped superconductivity and electronic structural evolution in tungsten ditelluride *Nat. Commun.* **6** 7805.

[6] D Kang, et al. 2015 Superconductivity emerging from a suppressed large magnetoresistant state in tungsten ditelluride *Nat. Commun.* **6** 7804.

[7] A A Soluyanov, D Gresch, Z Wang, Q Wu, M Troyer, X Dai, B A Bernevig 2015 Type-II Weyl semimetals *Nature* **527** 495-498.

[8] Y Wu, D Mou, N H Jo, K Sun, L Huang, S L Bud'ko, P C Canfield, A Kaminski 2016 Observation of Fermi arcs in the type-II Weyl semimetal candidate WTe_2 *Phys. Rev. B* **94** 121113.

[9] F Y Bruno, et al. 2016 Observation of large topologically trivial Fermi arcs in the candidate type-II Weyl semimetal WTe_2 *Phys. Rev. B* **94** 121112.

[10] C Wang, et al. 2016 Observation of Fermi arc and its connection with bulk states in the candidate type-II Weyl semimetal WTe_2 *Phys. Rev. B* **94** 241119.

[11] E Zhang, et al. 2017 Tunable Positive to Negative Magnetoresistance in Atomically Thin WTe_2 *Nano Lett.* **17** 878.

[12] V Fatemi, Q D Gibson, K Watanabe, T Taniguchi, R J Cava, P Jarillo-Herrero 2017 Magnetoresistance and quantum oscillations of an electrostatically tuned semimetal-to-metal transition in ultrathin WTe_2 *Phys. Rev. B* **95** 041410(R).

[13] L Wang, I Gutiérrez-Lezama, C Barreteau, D-K Ki, E Giannini, A F Morpurgo 2016 Direct

Observation of a Long-Range Field Effect from Gate Tuning of Nonlocal Conductivity *Phys. Rev. Lett.* **117** 176601.
[14] Z Fei, T Palomaki, S Wu, W Zhao, X Cai, B Sun, P Nguyen, J Finney, X Xu, D H Cobden 2016 Topological insulator behavior in monolayer WTe_2 Preprint *ArXiv* 1610.07924
[15] Y Wang, et al. 2016 Gate-tunable negative longitudinal magnetoresistance in the predicted type-II Weyl semimetal WTe_2 *Nat. Commun.* **7** 13142.
[16] J Jiang, et al. 2015 Signature of strong spin-orbital coupling in the large nonsaturating magnetoresistance material WTe_2 *Phys. Rev. Lett.* **115** 166601.
[17] I Pletikosić, M N Ali, A V Fedorov, R J Cava, T Valla 2014 Electronic Structure Basis for the Extraordinary Magnetoresistance in WTe_2 *Phys. Rev. Lett.* **113** 216601.
[18] Y Wang, K Wang, J Reutt-Robey, J Paglione, M S Fuhrer 2016 Breakdown of compensation and persistence of nonsaturating magnetoresistance in gated WTe_2 thin flakes *Phys. Rev. B* **93** 121108(R).
[19] L Wang, I Gutierrez-Lezama, C Barreteau, N Ubrig, E Giannini, A F Morpurgo 2015 Tuning magnetotransport in a compensated semimetal at the atomic scale *Nat. Commun.* **6** 8892.
[20] B Amin, T P Kaloni, U Schwingenschlogl 2014 Strain engineering of WS_2, WSe_2, and WTe_2 *RSC Adv.* **4** 34561-34565.
[21] L Fei, W Jian, G Hong 2015 Negative differential resistance in monolayer WTe_2 tunneling transistors *Nanotechnology* **26** 175201.
[22] J Lenz, S Edelstein 2006 Magnetic sensors and their applications *IEEE Sens. J.* **6** 631-649.
[23] H B Dang, A C Maloof, M V Romalis 2010 Ultrahigh sensitivity magnetic field and magnetization measurements with an atomic magnetometer *Appl. Phys. Lett.* **97** 151110.
[24] Y Chen, S M Gillette, T Fitchorov, L Jiang, H Hao, J Li, X Gao, A Geiler, C Vittoria, V G Harris 2011 Quasi-one-dimensional miniature multiferroic magnetic field sensor with high sensitivity at zero bias field *Appl. Phys. Lett.* **99** 042505.
[25] L Wang, et al. 2013 One-dimensional electrical contact to a two-dimensional material *Science* **342** 614-617.
[26] T Taniguchi, K Watanabe 2007 Synthesis of high-purity boron nitride single crystals under high pressure by using Ba–BN solvent *J. Cryst. Growth* **303** 525-529.
[27] W-D Kong, S-F Wu, P Richard, C-S Lian, J-T Wang, C-L Yang, Y-G Shi, H Ding 2015 Raman scattering investigation of large positive magnetoresistance material WTe_2 *Appl. Phys. Lett.* **106** 081906.
[28] P L Cai, J Hu, L P He, J Pan, X C Hong, Z Zhang, J Zhang, J Wei, Z Q Mao, S Y Li 2015 Drastic pressure effect on the extremely large magnetoresistance in WTe_2: quantum oscillation study *Phys. Rev. Lett.* **115** 057202.
[29] Z Zhu, X Lin, J Liu, B Fauqué, Q Tao, C Yang, Y Shi, K Behnia 2015 Quantum oscillations, thermoelectric coefficients, and the Fermi surface of semimetallic WTe_2 *Phys. Rev. Lett.* **114** 176601.
[30] F-X Xiang, M Veldhorst, S-X Dou, X-L Wang 2015 Multiple Fermi pockets revealed by Shubnikov-de Haas oscillations in WTe_2 *Europhys. Lett.* **112** 37009.
[31] Y Wu, N H Jo, M Ochi, L Huang, D Mou, S L Bud'ko, P C Canfield, N Trivedi, R Arita, A Kaminski 2015 Temperature-induced Lifshitz transition in WTe_2 *Phys. Rev. Lett.* **115** 166602.
[32] X-C Pan, et al. 2016 Carrier balance and linear magnetoresistance in type-II Weyl semimetal WTe_2 *Front. Phys.* **12** 127203.
[33] P K Das, et al. 2016 Erratum: Layer-dependent quantum cooperation of electron and hole states in the anomalous semimetal WTe_2 *Nat. Commun.* **7** 11355.

[34] C M Hurd 1972 The Hall Effect in Metals and Alloys, Springer, Berlin.

[35] J-H Chen, C Jang, S.Xiao, M.Ishigami, M.S.Fuhrer 2008 Intrinsic and extrinsic performance limits of graphene devices on SiO_2 *Nat. Nanotechnol.* **3** 206 - 209.

[36] Y Li, Z Wang, Y Lu, X Yang, Z Shen, F Sheng, C Feng, Y Zheng, Z-A Xu 2016 Negative Magnetoresistance in Topological Semimetals of Transition-Metal Dipnictides with Nontrivial Z2 Indices Preprint *ArXiv* 1603.04056

[37] Z Wang, Y Li, Y Lu, Z Shen, F Sheng, C Feng, Y Zheng, Z Xu 2016 Topological phase transition induced extreme magnetoresistance in $TaSb_2$ Preprint *ArXiv* 1603.01717

[38] Y Zhang, et al. 2016 Electronic Evidence of Temperature-Induced Lifshitz Transition and Topological Nature in $ZrTe_5$ Preprint *ArXiv* 1602.03576

[39] L Li, Y Yu, G J Ye, Q Ge, X Ou, H Wu, D Feng, X H Chen, Y Zhang 2014 Black phosphorus field-effect transistors *Nat. Nanotechnol.* **9** 372-377.

[40] B Radisavljevic, A Kis 2013 Mobility engineering and a metal–insulator transition in MoS_2 *Nat. Mater.* **12** 812.

[41] K Kaasbjerg, K S Thygesen, K W Jacobsen 2012 Phonon-limited mobility in n-type single-layer MoS_2 from first principles *Phys. Rev. B* **85** 115317.

[42] Y Zhang, Y-W Tan, H L Stormer, P Kim 2005 Experimental observation of the quantum Hall effect and Berry's phase in graphene *Nature* **438** 201-204.

[43] N A Mazhar, S Leslie, X Jun, F Steven, G Quinn, H Max, N P Ong, R J Cava 2015 Correlation of crystal quality and extreme magnetoresistance of WTe_2 *Europhys. Lett.* **110** 67002.

[44] S Hikami, A I Larkin, Y Nagaoka 1980 Spin-orbit Interaction and magnetoresistance in the 2D system *Prog. Theor. Phys.* **63** 707.

[45] A T Neal, H Liu, J Gu, P D Ye 2013 Magneto-transport in MoS_2: Phase Coherence, Spin–Orbit Scattering, and the Hall Factor *ACS Nano* **7** 7077.

[46] J Hu, et al. 2015 Enhanced electron coherence in atomically thin Nb_3SiTe_6 *Nat. Phys.* **11** 471-476.

Supporting Information for

Gate Tunable Magneto-resistance of Ultra-Thin WTe_2 Devices

Xin Liu[1*], Zhiran Zhang[1], Chaoyi Cai[1], Shibing Tian[1], Satya Kushwaha[2], Hong Lu[1], Takashi Taniguchi[3], Kenji Watanabe[3], Robert J. Cava[2], Shuang Jia[1,4*], Jian-Hao Chen[1,4*]

[1] International Center for Quantum Materials, Peking University, Beijing 100871, China

[2] Department of Chemistry, Princeton University, Princeton, USA

[3] High Pressure Group, National Institute for Materials Science, 1-1 Namiki, Tsukuba, Ibaraki 305-0044, Japan

[4] Collaborative Innovation Center of Quantum Matter, Beijing 100871, China

[*] Xin Liu (liux23@pku.edu.cn), Shuang Jia (jiashuang@gmail.com) and Jian-Hao Chen (chenjianhao@pku.edu.cn)

S1. Characteristics of a Bulk WTe_2 Crystal.

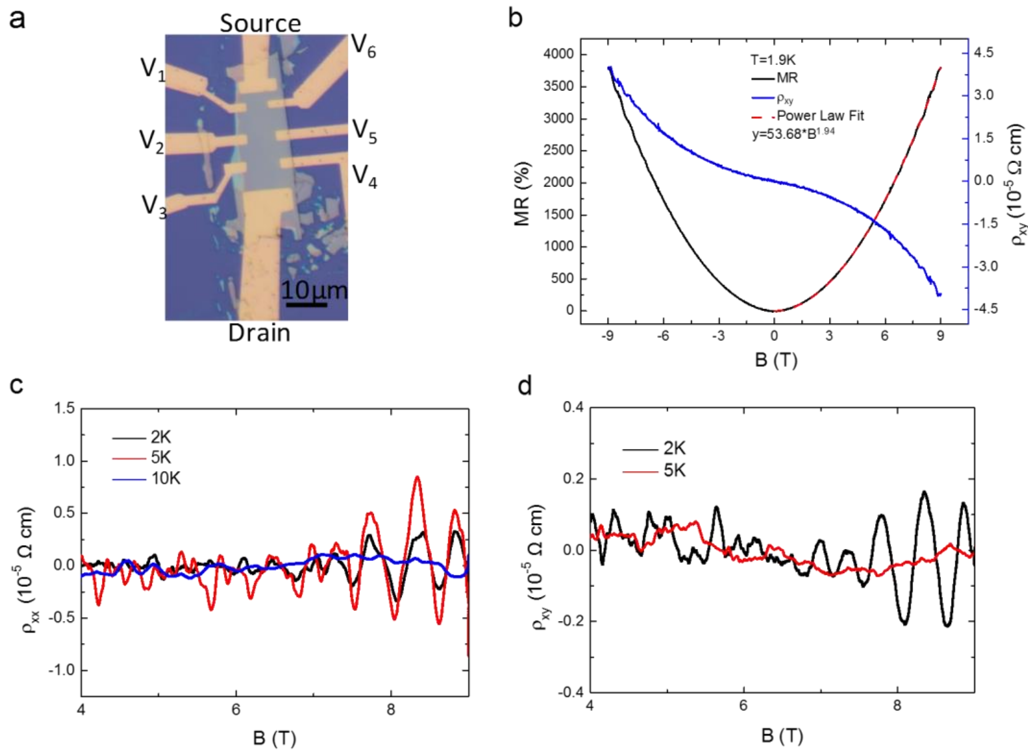

Figure S1a shows the optical image of ~112nm-thick WTe_2 FET device (sample B) which is mechanically exfoliated onto Si substrate with 300nm SiO_2. The source-drain current flows along the a-axis and the magnetic field is parallel to the c-axis. Longitudinal resistance ρ_{xx} is measured with probes V_1 and V_3, while Hall resistance ρ_{xy} is measured with probes V_1 and V_6. Magnetic field dependence and Hall resistance of the 112nm-thick WTe_2 crystal are shown in figure S1b. The MR of the measured device is up to 4000% under applied magnetic field of 9T

and the residual resistivity ratio (RRR) is about 58.39 at B=0T. Furthermore, we make a power law fit to MR and the exponent is about 1.94[1, 2]. Shubnikov–de Haas oscillations are observed both in ρ_{xx} and ρ_{xy} shown in figure S1c and S1d, which suggests that the quality of the thicker sample is good. The colors mark different temperatures.

S2. Temperature Dependence of Mobility in Bulk WTe_2 Crystals.

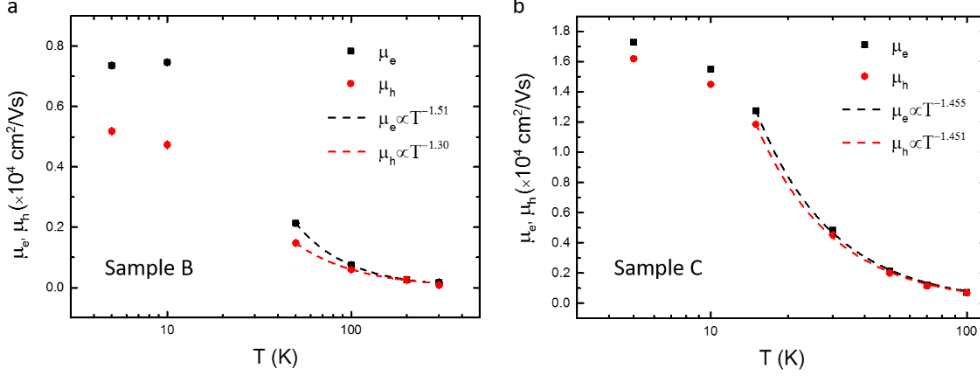

Figure S2 shows the dependence of mobilities u_e and u_h of sample B and C, respectively, as a function of temperature. Sample C is about 120nm thick and exfoliated from bulk WTe_2 crystal, whose growth process is different from sample B. Both mobilities for electron and hole of sample B in panel S2a increase following a power law fit of $\mu \propto T^{-\alpha}$ from 300K to 50K (100K to 15K, sample B in panel S2b) and then saturate from 10K to 2K (10K to 2K, sample B in panel S2a). A fit to a power law behavior of the decreasing mobility with increasing temperature give a larger exponent α for electrons (α=1.51, 1.455) and holes (α=1.30, 1.451) than WTe_2 thin flakes (α=0.61 for electrons and α=0.48 for holes) in the main text. Such values are close to the theoretically predicted value for bulk samples α～1.52.

A lower α in ultra-thin WTe_2 crystals means that such samples could preserve their low temperature mobilities much better than their bulk counterparts at higher temperatures. The two-fluid model provides a strong correlation between higher charge carrier mobility and larger magnitude of the XMR of the samples. Such correlation is also observed in experiments on bulk WTe_2 [3]. Thus a lower α at ultra-thin WTe_2 means that the ultra-thin samples could preserve their response to magnetic field much better than their bulk counterparts at room temperature.

S3. Raman Spectra of the Few-layer and Bulk WTe_2 Devices.

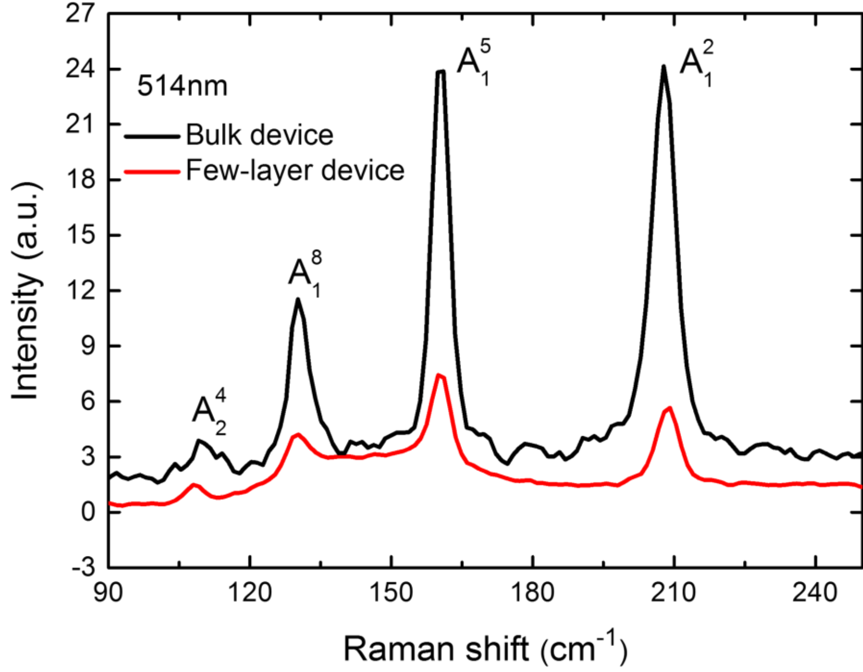

Figure S2 shows Raman spectra of the few-layer (sample A, in the main text) and 112nm-thick WTe_2 devices (sample B). Measurements are performed in a Horiba Jobin Yvon LabRam HR Evolution system. And we choose a non-polorized laser with wavelength of 514 nm at room temperature after accomplishing the transport experiments. Four prominent peaks are observed whose positions are A_1^2=209.14, A_1^5=159.96, A_1^8=130.306 and A_2^4= 107.995, respectively. The position in few-layer WTe_2 device is close to that in bulk materials (whose positions are A_1^2=207.8, A_1^5=159.845, A_1^8=130.19 and A_2^4= 109.12). The four Raman peaks suggest the measured WTe_2 samples are in 1T' phase [4] and it has not degraded.

S4. Gate Dependence of Mobility in WTe_2 Thin Flakes on Different Substrate.

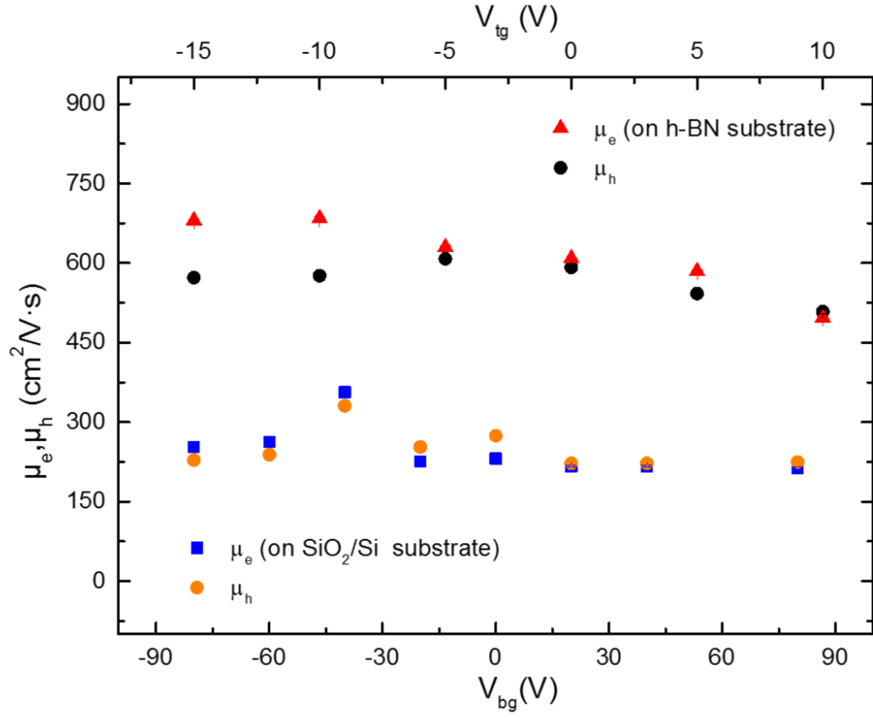

The gate dependence of mobility in WTe_2 devices (sample D and sample E) at T=2K is shown in Figure S3. WTe_2 thin flakes are mechanically exfoliated from bulk WTe_2 crystal and transferred on to thin h-BN single crystals (sample D) and SiO_2/Si substrates (sample E), respectively. Sample D is about 6-nm thick and sample E on the SiO_2/Si substrates is about 10-nm thick. There is an apparent increase in the mobility in device on h-BN substrate. In addition, better contact is achieved in thinner WTe_2 crystals on h-BN single crystal than on SiO_2/Si substrates.

S5. Gate Dependence of ρ_{xx} under Different In-plane Magnetic Fields.

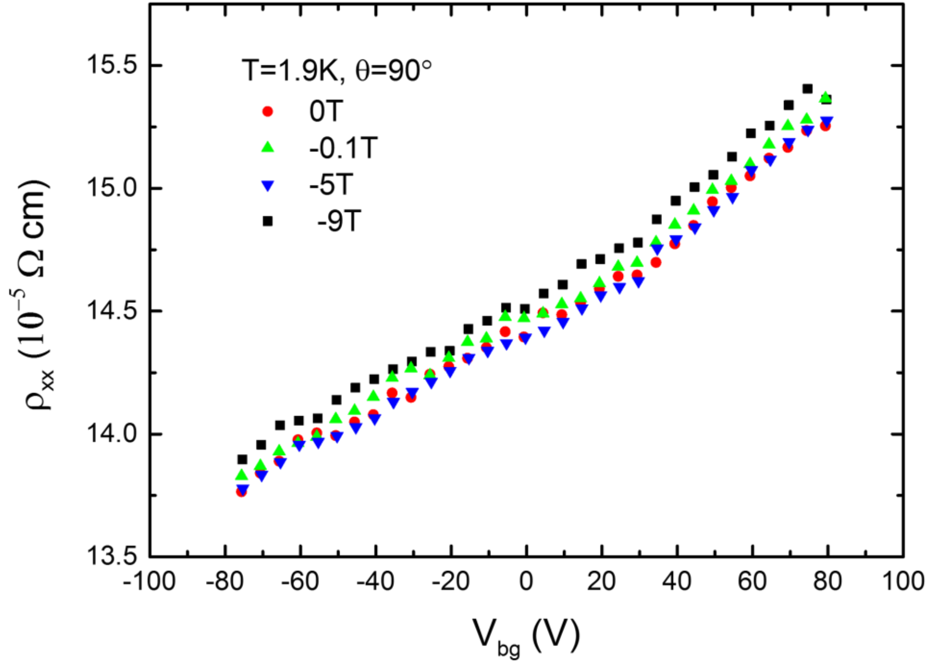

The gate dependence of longitudinal resistance of sample A at temperature of 1.9 Kelvin under various in-plane magnetic fields is shown in Figure S3. We find very little MR in the in-plane magnetic field, which is similar to that in bulk materials [5].

S6. Temperature Dependence of Longitudinal Resistance.

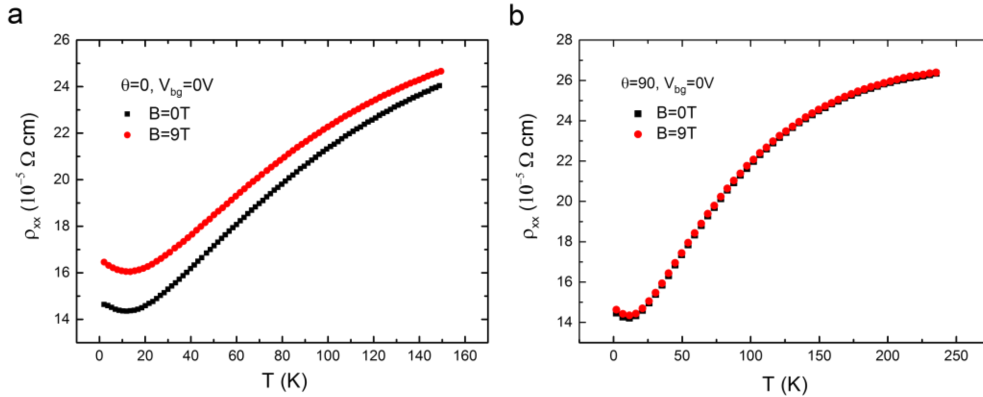

Figure S4 shows temperature dependence of longitudinal resistance of sample A under 0T and 9T magnetic field with zero back gate voltage. In figure S4a, magnetic field is applied perpendicular to the a-axis. We see a small increase in resistivity below 12K at zero magnetic field for our device, and the application of 9T magnetic field does not move the turn-on temperature T* much higher, which is likely caused by the suppression of MR in few-layer WTe_2 crystals. When the magnetic field is parallel to the ab plane (Fig. S4b), the MR is minimal for the whole temperature range of 1.9K to 250K.

S7. Magnetic Field Dependence of Power-Law-Fit Exponent

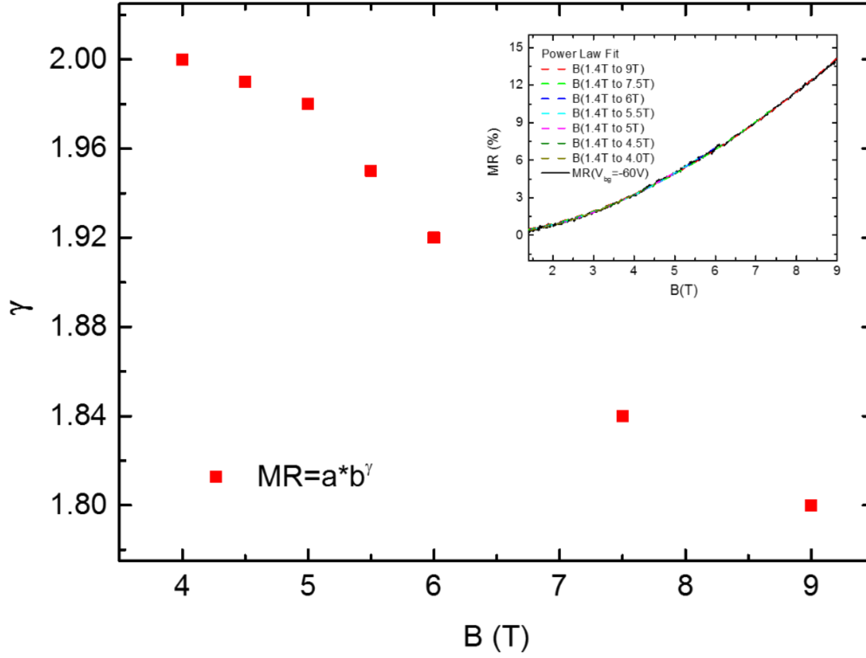

Figure S7 shows the power law fitting $MR \sim B^{\gamma}$ at different range of magnetic field for an experimental MR curve at back gate voltage -60V. It is seen in the inset panel that by fitting the MR between 1.4T and 4.0T, we obtained an exponent gamma=2; for MR between 1.4T and 6T, we obtained gamma=1.92; for MR between 1.4T and 9T, we obtained gamma=1.8. The fitting shows that the exponent γ is not a constant of magnetic field, and reveals the trend of saturation of MR at high enough magnetic field. Furthermore, this shows that the simple mathematical expression ($MR \sim B^{\gamma}$) might not capture the physics and we use the two fluid model to fit and understand the experimental data in the main text.

S8. Linear Extrapolation of Carrier Density and Mobility

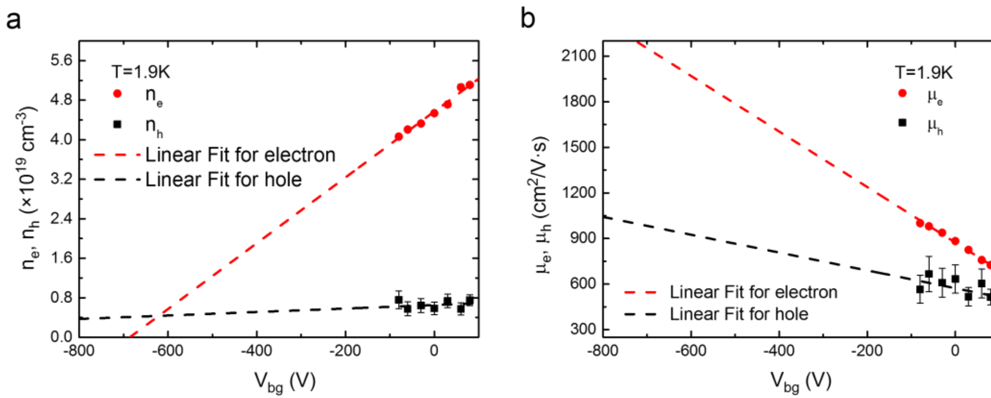

Figure S8 shows carrier density and mobility as a function of back gate voltage at temperature of 1.9 Kelvin. Dashed lines are linear fit to the experimental data, with specific parameters shown in equation (S1) to (S4). The linearity of our data is very good in the experimentally explored regime. We extend the linear extrapolation in n_e and n_h vs V_g and find that neutrality

will be obtained at V_{bg}=-620V (Figure S8a). To estimate the MR at neutrality for our device, we extend the linear extrapolation in μ_e and μ_h vs V_g at V_{bg}=-620V and obtain a change of MR to be 8,400%.

$$n_e = 6.67 \times 10^{-3} + 4.57\mathrm{V}_{bg} \quad (1)$$

$$n_h = 3.52 \times 10^{-4} + 0.65\mathrm{V}_{bg} \quad (2)$$

$$\mu_e = 873.26 - 1.83\mathrm{V}_{bg} \quad (3)$$

$$\mu_h = 572.43 - 0.58\mathrm{V}_{bg} \quad (4)$$

If the mobility of pristine bulk sample (as high as 167,000 $cm^2V^{-1}s^{-1}$ from ref.[3]) can be preserved, when the carrier density is adjusted from p/n=0.1599 to p/n=1, we use the constant mobility value (167,000 $cm^2V^{-1}s^{-1}$) to obtain a lower bound for the change of MR in such device to be 402,600%. Such rapid improvement of device fabrication techniques has been seen in the field of graphene, where it did not take a long time for the mobilities of graphene devices to improve from 10,000cm^2/Vs [6] to 1,000,000cm^2/Vs [7].

S9. Simultaneous Fitting of ρ_{xx} and ρ_{xy} Curves with the Least Squares Method

The two-fluid model gives:

$$\rho_{xx} = \frac{1}{e}\frac{(n_e u_e + n_h u_h) + (n_e u_h + n_h u_e) u_e u_h B^2}{(n_e u_e + n_h u_h)^2 + \left((n_e - n_h) u_e u_h B\right)^2} \quad (5)$$

$$\rho_{xy} = \frac{1}{e}\frac{(n_e \mu_e^2 - n_h \mu_h^2) - (n_h - n_e)\mu_e^2 \mu_h^2 B^2}{(n_e u_e + n_h u_h)^2 + \left((n_h - n_e) u_e u_h B\right)^2} B \quad (6)$$

where n_e (n_h) and u_e (u_h) are carrier density and mobility for electrons (holes), respectively. Here, we need to minimize the goodness-of-fit of between the experimental data of ρ_{xx} (ρ_{xy}) and theoretical curve from equation (S5) ((S6)) at each gate voltage and temperature.

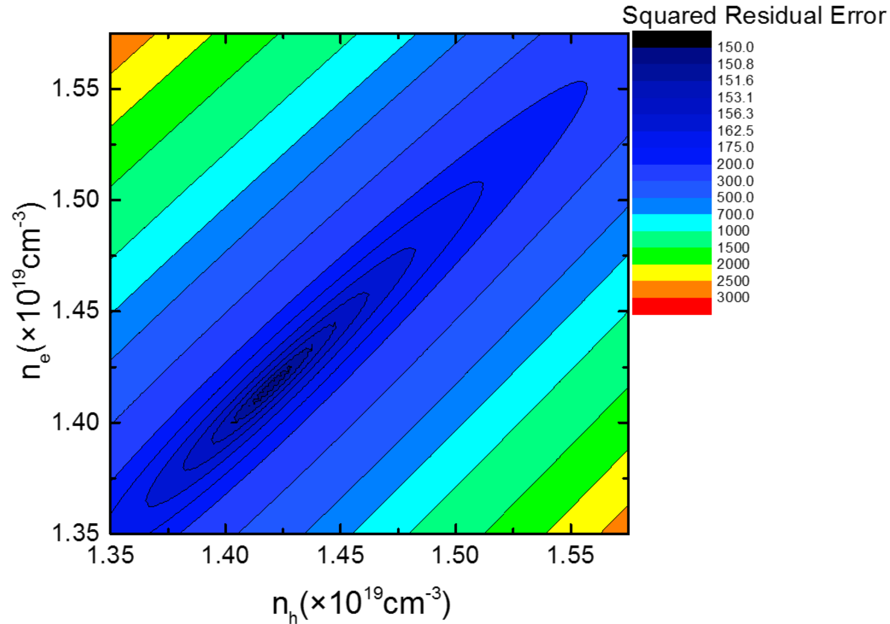

We first calculate the squared error of ρ_{xx} at a specific gate voltage and temperature. Since it is a function of four parameters, n_e, n_h, u_e, u_h, which could not be plotted in a straightforward way, we first determine the least squared error surface in this 4-dimensional parameter space with

the optimal μ_h and μ_e for each (n_h, n_e); e.g., we minimize the error for each point of (n_h, n_e) with the best μ_h and μ_e. Such least squared error surface could be drawn with n_h (X axis) and n_e(Y axis) and the squared error (Z axis). Then we use the same set of n_e, n_h, u_e, u_h to obtain the least squared error surface of ρ_{xy}. The joint least squared error of ρ_{xx} and ρ_{xy} versus n_h and n_e will be graphs similar to figure S6 (Figure S9 is obtained for V_g = 0V and T = 2K). Now we can determined the optimal n_h, n_e, μ_h and μ_e for each V_g and T from the point of such graphs that has the minimum squared error.

Reference:

[1] Y Wang, K Wang, J Reutt-Robey, J Paglione, M S Fuhrer 2016 Breakdown of compensation and persistence of nonsaturating magnetoresistance in gated WTe_2 thin flakes *Phys. Rev. B* **93** 121108(R).

[2] W. K. Kwok, L R Thoutam, Y L Wang, Z L Xiao, S Das, A Luican-Mayer, R Divan, G W Crabtree, W K Kwok 2015 Temperature-dependent three-dimensional anisotropy of the magnetoresistance in WTe_2 *Phys. Rev. Lett.* **115** 046602.

[3] N A Mazhar, S Leslie, X Jun, F Steven, G Quinn, H Max, N P Ong, R J Cava 2015 Correlation of crystal quality and extreme magnetoresistance of WTe_2 *Europhys. Lett.* **110** 67002.

[4] W-D Kong, S-F Wu, P Richard, C-S Lian, J-T Wang, C-L Yang, Y-G Shi, H Ding 2015 Raman scattering investigation of large positive magnetoresistance material WTe_2 *Appl. Phys. Lett.* **106** 081906.

[5] M N Ali, et al. 2014 Large, non-saturating magnetoresistance in WTe_2 *Nature* **514** 205.

[6] Y Zhang, Y-W Tan, H L Stormer, P Kim 2005 Experimental observation of the quantum Hall effect and Berry's phase in graphene *Nature* **438** 201-204.

[7] L Wang, et al. 2013 One-dimensional electrical contact to a two-dimensional material *Science* **342** 614-617.